Available online at www.sciencedirect.com

ScienceDirect

Journal of Nutritional Biochemistry 115 (2023) 109307

Journal of Nutritional Biochemistry

RESEARCH PAPER

Associations of altered hepatic gene expression in American lifestyle-induced obesity syndrome diet-fed mice with metabolic changes during NAFLD development and progression

Valeria Iannone[a,#], Johnson Lok[a,#], Ambrin Farizah Babu[a,b,#], Carlos Gómez-Gallego[a], Roosa Maria Willman[a,c], Ville Mikael Koistinen[a,b,d], Anton Klåvus[b], Mikko I. Kettunen[e], Anna Kårlund[a], Ursula Schwab[a,f], Kati Hanhineva[a,b,d,1,*], Marjukka Kolehmainen[a,2,*], Hani El-Nezami[a,g]

[a] School of Medicine, Institute of Public Health and Clinical Nutrition, University of Eastern Finland, Kuopio, Finland
[b] Afekta Technologies Ltd., Kuopio, Finland
[c] Department of Medicine, Institute of Biomedicine, University of Eastern Finland, Kuopio, Finland
[d] Department of Life technologies, Food Sciences Unit, University of Turku, Turku, Finland
[e] Kuopio Biomedical Imaging Unit, A.I. Virtanen Institute for Molecular Sciences, University of Eastern Finland, Kuopio, Finland
[f] Department of Medicine, Endocrinology and Clinical Nutrition, Kuopio University Hospital, Kuopio, Finland
[g] Molecular and Cell Biology Division, School of Biological Sciences, University of Hong Kong, Hong Kong China

Received 19 August 2022; received in revised form 20 January 2023; accepted 24 February 2023

Abstract

Non-alcoholic fatty liver disease (NAFLD) pathogenesis remains poorly understood due to the complex metabolic and inflammatory changes in the liver. This study aimed to elucidate hepatic events related to inflammation and lipid metabolism and their linkage with metabolic alterations during NAFLD in American lifestyle-induced obesity syndrome (ALIOS) diet-fed mice. Forty-eight C57BL/6J male mice were fed with ALIOS diet (n=24) or control chow diet (n=24) for 8, 12, and 16 weeks. At the end of each timepoint, eight mice were sacrificed where plasma and liver were collected. Hepatic fat accumulation was followed using magnetic resonance imaging and confirmed with histology. Further, targeted gene expression and non-targeted metabolomics analysis were conducted. Our results showed higher hepatic steatosis, body weight, energy consumption, and liver mass in ALIOS diet-fed mice compared to control mice. ALIOS diet altered expression of genes related to inflammation (*Tnfa* and *IL-6*) and lipid metabolism (*Cd36, Fasn, Scd1, Cpt1a*, and *Ppara*). Metabolomics analysis indicated decrease of lipids containing polyunsaturated fatty acids such as LPE(20:5) and LPC(20:5) with increase of other lipid species such as LPI(16:0) and LPC(16:2) and peptides such as alanyl-phenylalanine and glutamyl-arginine. We further observed novel correlations between different metabolites including sphingolipid, lysophospholipids, peptides, and bile acid with inflammation, lipid uptake and synthesis. Together with the reduction of antioxidant metabolites and gut microbiota-derived metabolites contribute to NAFLD development and progression. The combination of non-targeted metabolomics with gene expression in future studies can further identify key metabolic routes during NAFLD which could be the targets of potential novel therapeutics.

Keywords: Non-alcoholic fatty liver disease (NAFLD); NAFLD pathogenesis; Non-targeted metabolomics analysis; Lipid metabolism; Inflammatory markers.

* Corresponding authors: School of Medicine, Institute of Public Health and Clinical Nutrition, University of Eastern Finland, 70200, Kuopio, Finland.
E-mail addresses: kati.hanhineva@uef.fi (K. Hanhineva), marjukka.kolehmainen@uef.fi (M. Kolehmainen).
# These authors contributed equally.
1 Tel.: +358403552364.
2 Tel.: +358 40 355 3617.

https://doi.org/10.1016/j.jnutbio.2023.109307

1. Introduction

Worldwide, non-alcoholic fatty liver disease (NAFLD) is the most common chronic liver disease and affects about 25% of the world's population [1]. NAFLD is defined as excessive hepatic fat accumulation in individuals consuming little or no alcohol [2]. Moreover, NAFLD patients can exhibit a wide range of liver conditions ranging from simple steatosis to steatohepatitis and liver cirrhosis [3]. Furthermore, NAFLD is associated with abnormal glucose metabolism and plasma lipid profile, and NAFLD patients have a higher risk of type II diabetes, cardiovascular diseases, and chronic kidney disease (2-fold higher risk) [4,5].

An unhealthy lifestyle, including sedentary behavior and increased energy intake, contributes towards the rising occurrence of NAFLD [6]. Consumption of the Western diet consisting of sources of low fiber carbohydrates, saturated fat, and fructose, represents a public health concern as they can predispose individuals to metabolic diseases such as obesity and type II diabetes, in addition to NAFLD [6–8].

Although several studies have proposed to explain NAFLD pathogenesis and its progression to non-alcoholic steatohepatitis (NASH), gaps still remain in understanding the molecular and metabolic events related to both the development and progression. The early stage called simple steatosis or non-alcoholic fatty liver (NAFL) is characterized by an excessive amount of lipid accumulation in the liver [3,9]. Alterations in lipid metabolism such as changes in the fatty acids and phospholipid composition in the liver samples of NAFLD patients suggest that lipid metabolism is a key player in the pathogenesis of NAFLD [10,11].

The mechanisms that mainly regulate hepatic lipid metabolism include fatty acid uptake, *de novo* lipogenesis, and fatty acid β-oxidation [12]. Simple steatosis may be followed by NASH, where reactive oxygen species (ROS) are produced due to the increased hepatic free fatty acid oxidation [3,9]. These alterations observed in the liver in turn induce the release of pro-inflammatory signals, such as tumor necrosis factor alpha (TNFα) and activation of hepatic stellate cells, eventually causing fibrosis [3,9]. This may then progress to an irreversible stage called cirrhosis and ultimately lead to hepatocellular carcinoma [3,9].

Different animal models have been widely used to study the mechanisms of NAFLD pathogenesis including mice undergoing diet intervention such as "*The American lifestyle-induced obesity syndrome diet*" (ALIOS) which has been shown to recapitulate the clinical and transcriptomic features observed in NAFLD and NASH patients [13]. Therefore, here, we used mice fed with the ALIOS diet for studying specifically the early events of NAFLD. The present study aimed to better elucidate the events occurring in the liver during NAFLD development when the NAFLD condition is still reversible at 8, 12, and 16 weeks of ALIOS diet intervention. We applied non-targeted metabolomics technology to identify NAFLD-associated metabolic changes and key metabolic pathways that are altered upon ALIOS diet intervention. The metabolomics findings were further correlated with gene expression changes in the markers of inflammation and lipid metabolism measured in the liver samples to identify crucial altered pathways during NAFLD development.

2. Materials and methods

2.1. Animals and study design

The experimental protocol for the study was approved by the National Ethics Committee for Animal Experiments in Finland (license number: ESAVI/21371/2019) and conformed to the regulations and requirements of the European Union concerning the protection of animals used for scientific purposes. The study was performed and reported according to the ARRIVE guidelines [14]. Five to 6-week-old male C57BL/6J (Jackson Laboratory, Bar Harbor, Maine, USA) mice were housed in the animal housing facilities at the University of Eastern Finland and were kept under specific-pathogen-free conditions in individually ventilated cages (16.62 cm x 32.5 cm x 9.9 cm) with 4 mice per cage under a 12/12 h light cycle at 20.5°C (±0.2°C) with humidity at 54.6% (±3.9%). All mice were earmarked for individual follow-up. Forty-eight mice were acclimatized for 2 weeks and were subsequently divided into 2 groups. Twenty-four mice were fed with the ALIOS diet (trans fat custom diet TD.06303 with 22% by weight of fat from hydrogenated vegetable oil, Envigo, Madison, Wisconsin USA, www.envigo.com) with high-fructose corn syrup (HFCS) equivalent (45% glucose and 55% fructose by weight) at 42 g/L in their drinking water [15]. Twenty-four mice were fed with the control diet (AIN-93M Purified Diet TD.94048, Envigo, Madison, WI, USA, www.envigo.com). Further details on the diet compositions are described in the Supplementary file 1 and Supplementary Table 3. Mice were sacrificed after 8, 12, and 16 weeks of the diet intervention respectively and samples were collected. Cages were randomized by drawing lots and assigned to the different diet treatments and sacrifice timepoints. The number of mice per group per timepoint was calculated with the Power Analysis equation using the "G*Power" program [16,17] based on previously reported results [15]. Mice were weighed weekly. The diet and high-fructose corn syrup (HFCS) equivalent water consumption were both recorded three times per week by measuring the weight of the diet and water remaining and added. The energy consumption of control mice was calculated as 3.6 kcal per gram of control diet consumed. Energy consumption of ALIOS diet-fed mice was calculated as 4.6 kcal per gram of ALIOS diet and 0.15 kcal per gram of HFCS water consumed. Data presented as energy consumption per mice per day was estimated by dividing the weekly energy consumption per cage by four and then by seven. At the end of the dietary intervention, mice were placed under anesthesia with isoflurane. Following deep anesthesia, the heart blood sample was collected via cardiac puncture and the mice were terminated using cervical dislocation. Four mice fed with the control diet were excluded from the analysis (Supplementary File 3). The livers were collected and weighted immediately. Liver weights were expressed as mg per 100mg body weight.

2.2. Plasma NAFLD biomarkers

Plasma samples were immediately separated from the whole blood using plasma tubes with separating gel and lithium heparin (Category number: 365986, Becton, Dickinson and Company, Franklin Lakes, NJ, USA) according to the manufacturer's instructions, aliquoted, and frozen in liquid nitrogen before being stored in -80°C. Plasma concentrations of alanine aminotransferase (ALT) and aspartate aminotransferase (AST) were measured by the automated clinical chemistry analyzer Konelab Prime 60 using the Modified International Federation of Clinical Chemistry and Laboratory Medicine (IFCC)-standard method [18,19].

2.3. Magnetic resonance imaging (MRI)

MRI was performed to quantify the liver fat content for confirming the development of NAFLD before the sacrifice at time points weeks 8, 12, and 15. 4 mice per group (ALIOS diet-fed and control mice) were used for MRI analysis at weeks 8, 12, and 15. To allow time for the mice to recover from anesthesia required for the MRI procedure, mice that underwent MRI at week 8 were eventually sacrificed at week 12. Mice that underwent MRI at week 12 were similarly sacrificed at week 16. Lastly, mice that underwent MRI at week 15 were sacrificed at week 16, after 1 week of recovery from MRI procedure.

The methodology for performing MRI analysis was adapted from previous methods [20,21]. To quantify liver fat content using MRI, the mice were anesthetized with isoflurane (5% induction, 1.5% maintenance). Imaging was performed at 7 T (Pharmascan, Bruker Biospin, Ettlingen, Germany) using a quadrature volume coil transmitter and a quadrature rat head surface coil receiver (Rapid Biomedical, Rimpar, Germany). Breathing-gated 3D gradient echo pulse sequence (repetition time 40 ms, echo time 3.8 ms, field of view 3.2×2.1×2.2 cm collected with an isotropic resolution of 250 μm, saturation slabs outside the field of view were used to avoid unwanted signal) with a sequential frequency-selective excitation (5.5 ms gauss-pulse with a nominal flip angle of 30 degrees) of water (0 Hz) and fat (-1051 Hz) resonance for each repetition time. In one animal, from the control mice at timepoint week 12, apparent T_1 relaxation times of liver water and subcutaneous fat signals were also measured using inversion recovery Rapid Imaging with Refocused Echoes (RARE) pulse sequence (inversion times 100 ms and 6400 ms, repetition time 8 s, echo time 4.5ms, 16 echoes, single 1mm slice with 3.2×2.4 cm field of view collected with 250 μm isotropic resolution). MRI fat index measured as fat-to-total-signal ratio was estimated as Eq. (1)

$$\frac{S_{FAT}}{S_{FAT} + S_{WATER}} \quad (1)$$

using a home-built Matlab script (Natick, MA, USA). Fat and water signals have different T_1 relaxation times leading to a difference in their signal saturation. Based on the used sequence parameters and measured T_1 relaxation times (water 1.1 s, fat 0.6 s), the steady-state fat signal is 50% higher than water, which was considered when calculating the ratio. A constant correction factor of 1.5 was used throughout the analysis.

2.4. Liver histology

Liver samples for histology were collected from the left lateral lobe and fixed overnight in 4% paraformaldehyde (Sigma-Aldrich, Germany, PFA) in phosphate buffered saline (Phosphate Buffer Saline 1X, Lonza, PBS) 1X at +4°C. Tissues were stored in ethanol 70% at +4°C until the processing. The samples were processed with an automated tissue processor (Thermo Scientific Citadel 2000, MA, USA), embedded into paraffin blocks, and cut 5μm tissue sections by microtome (Thermo Scientific HM 430 Sliding Microtome, MA, USA). Liver samples for histology and liver lipid quantification were collected from the left lateral lobe and fixed for 2 h in 4% PFA in PBS 1X, cryoprotected with a sucrose scale (10% and 20% for 40 min and 30% overnight), and included in OCT embedding medium (Thermo Fischer Scientific, MA, USA), frozen in isopentane-liquid nitrogen mixture, and stored at -80°C. The samples were cut into 8 μm thick cryosections by cryostat (Leica CM3050 S, Germany) and stored at -80°C until the staining. Haematoxylin and eosin (H&E) and Sirius red staining of liver paraffine-embedded samples were performed respectively for visual examination of morphological features and to assess fibrosis. Inflammatory loci in H&E liver sections defined as reported by Liang et al. [22], were observed in each tissue section. Samples from four ALIOS diet-fed mice and four control mice were randomly selected at 8, 12, and 16 weeks stained, and 8 images from each mouse were acquired using a microscope (Olympus BX51, Tokyo, Japan) with 10x objective.

2.5. Visualisation and quantification of liver lipid with Oil Red O staining

Oil Red O (ORO) staining was performed on frozen liver sections for the visualization of micro and macro steatosis and quantification of fat content. Samples from six ALIOS diet-fed mice and six control mice randomly selected at each timepoint (8, 12, and 16 weeks) respectively were stained. Eight images from each mouse were acquired using Olympus BX51 microscope (Olympus BX51 (Olympus, Tokyo, Japan) with 10x objective. Fiji (ImageJ) software version 1.52p was used for steatosis quantification in liver samples. Lipid droplets were segmented using Trainable Weka Segmentation plugin [23]. The Trainable Weka Segmentation and the trained classifier were applied for all the acquired images. The image was then converted into 8-bit binary and the "Default" threshold algorithm was applied. The area corresponding to lipid droplets was measured using the "Analyse particles" tool and particles from 0- to infinity ^2 size was considered in the analysis.

2.6. RNA analysis

To isolate RNA, liver tissue collected was immediately submersed in RNA stabilization solution (RNA later, Qiagen, Germany), frozen immediately in liquid nitrogen and stored at -80C. The tissue was homogenized in Buffer RLT (Qiagen, Germany) and extracted with RNeasy mini kit (Qiagen, Germany). The concentration of RNA was measured by microspectrophotometry (NanoDrop Technologies, Wilmington, DE, USA). Tumor necrosis factor (*Tnfa*), Interleukin 6 (*Il6*), Toll-like receptor 4 (*Tlr4*), Transforming growth factor beta (*Tgfb*), CD36 molecule (*Cd36*), acetyl-Coenzyme A carboxylase alpha (*Acaca*), Fatty Acid Synthase (*Fasn*), Stearoyl-CoA desaturase (*Scd1*), Carnitine palmitoyltransferase 1a (*Cpt1a*), Peroxisome Proliferator Activated Receptor alpha (*Ppara*) and Glyceraldehyde 3-phosphate dehydrogenase (*Gapdh*) mRNA were measured using QuantStudio 6 Real-Time PCR system (ThermoFisher Scientific, Waltham, MA, USA) and using SensiFAST SYBR Lo-ROX Kit (Meridian Life Science, Memphis, TN, USA). The primer sequences used are listed in Supplementary Table S1. The results were normalized to the GADPH expression gene. The results were quantified using 2^{-ddCT} method [24] and expressed as fold change relative to the control groups.

2.7. Statistical analysis

To compare ALIOS diet-fed mice and control mice at each time point (8, 12, and 16 weeks), statistical analysis for both body weight and energy consumption at each week was performed using an unpaired t-test with the Holm-Sidak method for correcting multiple comparisons using GraphPad (version 6.01). Statistical analysis for liver weight, ALT and AST levels, MRI fat index, quantification of ORO and Sirius Red staining, and gene expression quantification, were performed using one-way ANOVA with post hoc multiple comparisons with Bonferroni correction using GraphPad (version 6.01).

2.8. Metabolomics analysis

2.8.1. Sample preparation

The frozen liver samples were prepared according to Klåvus et al. [25] by adding 80% v/v aqueous HPLC grade methanol in a ratio of 500 μL per 100 mg of the sample followed by homogenizing using Bead Ruptor 24 Elite homogenizer at the speed 6 m/s at 0±2°C for 30 s. The samples were subsequently vortexed and filtered (Captiva ND filter plate 0.2 μm) by centrifuging for 10 min at 4°C with 20,000×g and kept at 4°C until analysis. Small aliquots of the analytical samples were combined to constitute the quality control (QC) sample. Additionally, a solvent blank (80% v/v aqueous HPLC grade methanol) was prepared in the same manner as the analytical samples.

2.8.2. LC-MS analyses

The liquid chromatography-mass spectrometry (LC-MS) analyses of the liver samples were performed according to Klåvus et al. [25]. Briefly, reversed phase (RP) LC (Vanquish Flex UHPLC system, Thermo Scientific, Bremen, Germany) coupled to high-resolution Orbitrap mass spectrometry (Q Exactive Focus, Thermo Scientific, Bremen, Germany) was used. An injection volume of 1 μL was employed using a Zorbax Eclipse XDB-C18 column (dimensions 2.1×100 mm, particle size 1.8 μm; Waters Corporation, USA). Further, hydrophilic interaction LC (HILIC) was performed on a 1290 Infinity Binary UPLC coupled with a 6540 UHD Accurate-Mass quadrupole time-of-flight (QTOF) MS (Agilent Technologies, CA, USA). Here, Aqcuity UPLC BEH amide column (2.1×100 mm, 1.7 μm; Waters Corporation, USA) with an injection volume of 3 μL was used. For both analytical setups, the data were acquired in both positive (ESI+) and negative (ESI−) electrospray ionization modes. Quality control samples were injected at the beginning of the analysis and after every 12 samples. Further details on the LC-MS instrument set-up and MS/MS analysis are described in Supplementary File 2.

2.8.3. Data analysis

After the collection of the raw measurement data, MS-DIAL (Version 4.18) [26] was employed for automated peak picking and alignment to constitute the data matrix subjected to pre-processing as follows: After fusion of the data from the four analytical modes, signals present in less than 50% of the samples in both the ALIOS diet-fed mice and control mice along with a detection rate of less than 20% of the pooled QC samples were excluded. Then, drift correction was employed to correct for intensity drifts induced by the LC-MS analytical sequence using methods described by Klåvus et al. [25]. After drift correction, low quality signals with high spread of QCs were flagged; to not get flagged, a signal was required to have RSD*<0.2 and D-ratio*<0.4 or RSD*<0.1, RSD <0.1 and D-ratio<0.1 [27]. Then, missing values in the high-quality signals were imputed using random forest imputation. For low-quality flagged signals, zero imputation was used instead.

All statistical analyses for metabolite signals were performed using R version 3.6.1 [28]. The differential metabolites in the ALIOS diet-fed mice and control mice across the different time points were identified by using a feature-wise linear model. Features were used as the dependent variable. The effects of the intervention, time, and their interaction were modelled predictors. The interaction term reflects the difference in changes during the intervention between the ALIOS diet-fed mice and control mice. Feature-wise tests were adjusted for multiple comparisons using the Benjamini Hochberg false-discovery rate method (FDR). FDR adjusted *P*-value < .05 was used as a criterion for further investigations and annotation of signals. Further, only those features which had an MS/MS spectrum and had an arbitrary value for the average peak area of at least 10,000 were addressed.

The chosen signals were annotated using MS-DIAL [26] by comparing the exact *m/z*, retention time, and MS/MS fragmentation patterns against our in-house standard library and publicly available spectral databases, such as MassBank [29] and MassBank of North America (https://mona.fiehnlab.ucdavis.edu/). Further, additional searches in online MS spectral databases [30–32] were also performed. Additionally, MS-FINDER [33] was used to characterize the unknowns. Moreover, the vendor software - Agilent MassHunter Qualitative Analysis B.07.00 and Thermo FreeStyle 1.3 were used for the exploration of raw data extracted ion chromatograms (EICs) and MS/MS fragmentation spectra. Following compound annotation, using in-house scripts in R Software (Version 3.6.2), the top 25 significantly different identified metabolites were used to plot a heatmap representing Spearman's correlations. Volcano plots of standardized effect size and FDR-adjusted *P*-values from the linear models were created. Bar plots representing the raw abundances of the significantly different metabolites were created using GraphPad (version 6.01) and the significance values were computed by one-way ANOVA with post hoc multiple comparisons with Bonferroni correction.

3. Results

3.1. ALIOS diet-fed mice had higher body weight, energy consumption, and liver mass compared to the control mice

Parameters describing the development of NAFLD including body weight, liver mass, and energy consumption were measured to follow NAFLD development. ALIOS diet-fed mice had statistically significant higher body weight compared to the control mice starting from week 2 (*P*=.0274) to 12 (*P*=.0395; Fig. 1A). ALIOS diet-fed mice at weeks 12 and 16 had a significant increase in liver weight compared to control mice (week 12: *P*=.0038; week 16: *P*=.0042; Fig. 1B). The liver weight of the control mice gradually increased over time (at week 8 was 1435 mg±316; at week 12 was

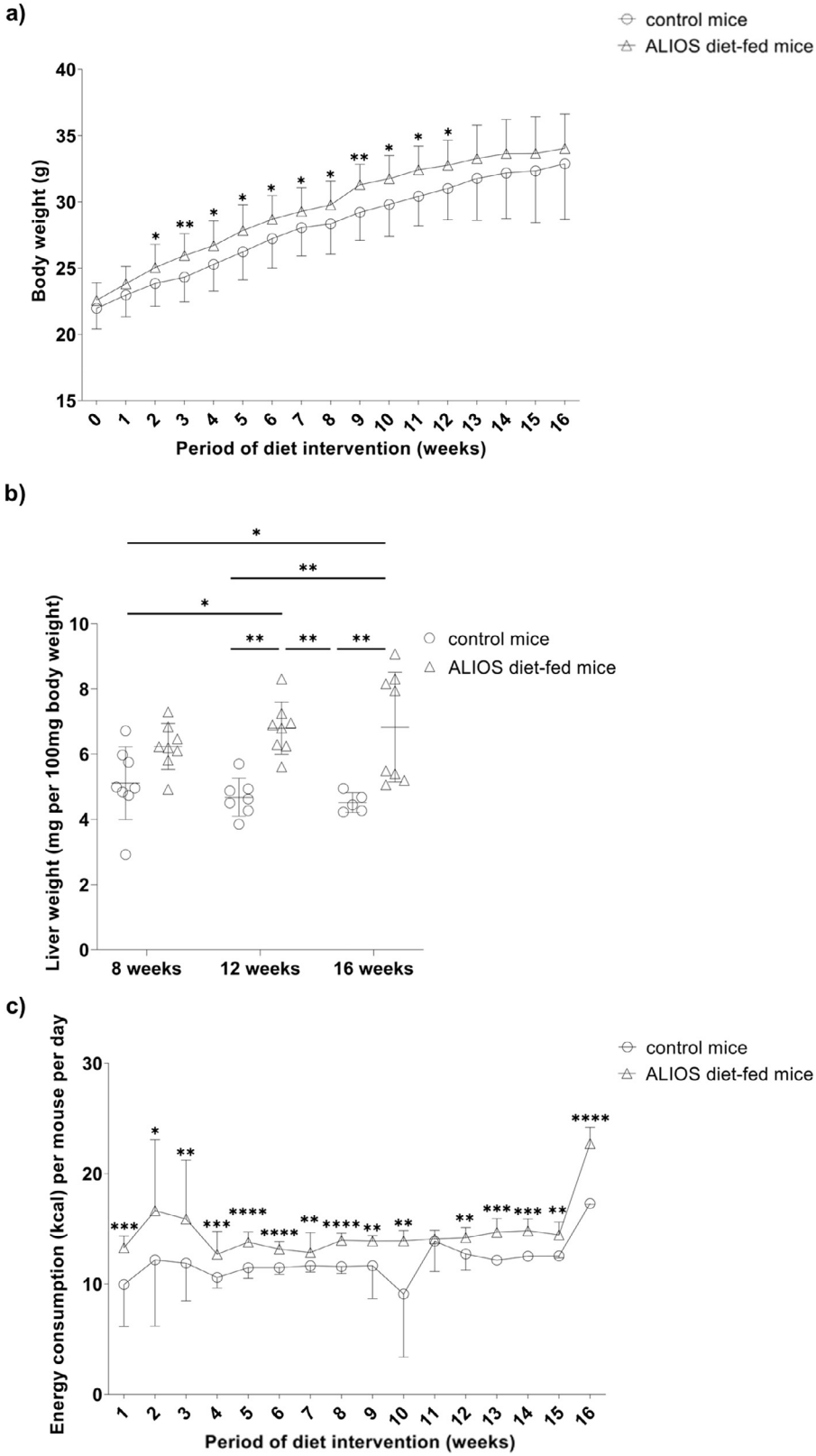

Fig. 1. (A) Body weight, (B) liver weight and (C) energy consumption in ALIOS diet-fed mice and control mice at week 8, 12 and 16 of diet intervention. For body weight and energy consumption, control mice (from week 0 to 8: n=20; week 9–12: n=12; week 13–16: n=5); ALIOS diet-fed mice (from week 0–8: n=24; week 9–12: n=16; week 13–16: n=8). Error bars indicate SD values (To avoid overlap of SD bars, only the upper SD bar in the ALIOS diet-fed mice group and the lower SD bar in the control mice group are shown). For liver weight, control mice at week 8 (n=8), week 12 (n=7), and week 16 (n=5); ALIOS diet-fed mice at week 8, 12 and 16 (n=8 for each time point) of diet intervention. Results are presented as average values where error bars denote SD. Statistical significance between different groups were shown using asterisks (* $P \leq .05$, ** $P \leq .01$, *** $P \leq .001$, **** $P \leq .0001$). ALIOS: American lifestyle-induced obesity syndrome.

1458 mg±177; and at week 16 was 1480 mg±192). ALIOS diet-fed mice also consumed significantly more energy per day compared to the control mice throughout the diet intervention period (Fig. 1C). Overall, though non-significant, ALIOS diet-fed mice had higher plasma ALT (at all timepoints; Supplementary Fig. S1A) and AST (week 8 and 12; Supplementary Fig. S1B) concentrations when compared to control mice.

3.2. Liver fat accumulation without fibrosis up to 16 weeks of ALIOS diet intervention

Histological examinations by H&E staining of the left lateral liver lobe in ALIOS diet-fed mice was performed to examine the liver lipid accumulation as a key sign of NAFLD development during the ALIOS diet intervention. The results demonstrated a progressive development of steatosis at different time points in ALIOS diet-fed mice compared to the control mice (Fig. 2). At week 8 in mice fed with the ALIOS diet, both macro and micro mild steatosis was observed in H&E staining, mostly in the periportal zone and absent around the central vein area (Fig. 2, Supplementary Fig. S2). While at 12 weeks of ALIOS diet, there was the presence of micro and macro steatosis, and fat droplet size of macro steatosis increased compared to control mice (Fig. 2). This difference between mice under ALIOS and control diet became visually more evident at 16 weeks of ALIOS diet (Fig. 2, Supplementary Fig. S2). Few inflammatory loci were observed at 12 and 16 weeks of ALIOS diet and were scattered into the tissue when assessed as described by Liang et al. [22] (Fig. 2). However, this was not observed at 8 weeks of ALIOS diet and in all control mice.

The percentage of fat droplets accumulating in the liver sections increased significantly ($P \leq .0001$) at 12 weeks of feeding ALIOS diet compared to control mice (Figs. 2 And 3A). This increase significantly persisted until the end of the study and the percentage of fat droplets quantified at 16 weeks in ALIOS diet-fed mice was statistically significant higher ($P \leq .0001$) compared to control mice. In addition, a significantly higher percentage of liver fat droplets was observed at 16 weeks in ALIOS diet-fed mice compared to ALIOS diet-fed mice after 8 weeks ($P \leq .0001$; Fig. 3A). Moreover, at 16 weeks, a mild but significant accumulation of fat droplets ($P=.0145$) in the liver in control mice was noted in comparison to the control mice at 8 weeks (Figs. 2 And 3A). ALIOS diet-fed mice at week 8 and 12 had significantly higher liver fat content ($P=.0039$ and $P=.0006$, respectively) compared to control mice using MRI, but the difference was statistically non-significant at week 15 (Fig. 3B And C). In addition, collagen-specific dye (Sirius Red) was used to assess the presence of fibrosis showing no evidence of collagen deposition either in ALIOS diet-fed or in control mice (at 8, 12, and 16 weeks, Fig. 2). *Tgfb* expression in mouse liver tissue was done for further confirmation of the Sirius Red staining observations and no differences were observed in the expression between the groups (ALIOS diet-fed mice and control mice) and along the time (weeks 8, 12, and 16; Supplementary Fig. S3J).

3.3. Genes related to hepatic inflammation and lipid metabolism showed altered expression

In this study, the expression of key genes involved in the inflammatory processes was altered in the liver after the diet intervention. *Tnfa* expression showed a gradual statistically significant increase of expression in ALIOS diet-fed mice at all time points compared to control mice ($P=.0048$ at week 8, $P=.0048$ at 12 weeks, and $P<.0001$ at 16 weeks of ALIOS diet-fed mice, respectively; Figure 4A-ii and 4C-ii, Supplementary Fig. S3A). *Il6* expression was not differential between mice under ALIOS and control diet at 8 weeks (Supplementary Fig. S3B). At 12 weeks, the expression of *Il6* in the control mice was higher ($P=.0073$) than in the mice under the ALIOS diet (Fig. 4B-ii, Supplementary Fig. S3B) and at 16 weeks of ALIOS diet, mice had higher ($P=.0393$) gene expression of the cytokine (Supplementary Fig. S3B).

Moreover, expression of key genes involved in regulating the hepatic lipid metabolism was shown to be altered in NAFLD occurrence including *Cd36, Acaca, Fasn, Scd1, Cpt1a*, and P*para*. In our study, ALIOS diet-fed mice had significantly higher expression of *Cd36* (4-fold increase; $P<.0001$) compared to control mice at all timepoints (Fig. 5B-ii, Supplementary Fig. S3D). At week 8, ALIOS diet-fed mice had significantly higher expression of *Fasn* ($P=.0017$) compared to control mice whereas its expression was significantly decreased in ALIOS diet-fed mice at week 12 ($P=.0399$; Fig. 5A-ii, Supplementary Fig. S3F). ALIOS diet-fed mice at all timepoints showed also significantly higher expression of *Scd1* compared to control groups ($P=.0002$ at 8 weeks, $P=.0218$ at 12 weeks and $P=.0093$ at 16 weeks of ALIOS diet-fed mice; Figure 5A-v and 5B-vi, Supplementary Fig. S3G). However, there were no statistically significant differences between the different timepoints in either of the diet groups for the expression of *Acaca, Fasn, Scd1*.

In addition, the gene expression analysis of *Cpt1a* and *Ppara* ALIOS diet-fed mice showed significantly higher expression of *Cpt1a* compared to control mice at week 8 ($P<.0001$) and week 16 ($P=.0092$; Supplementary Fig. S3H); while ALIOS diet-fed mice at week 8 had significantly higher expression ($P=.0002$) of *Ppara* but statistically non-significantly higher in week 12 and 16 when compared to control mice (Supplementary Fig. S3I). We also report a non-statistically significant trend of higher gene expression of *Tlr4* (week 12 and 16) and *Acaca* (week 8 and 12) in ALIOS diet-fed mice compared to control mice (Supplementary Fig. S3C).

3.4. ALIOS diet caused a switch in lipid and amino acid metabolism in the liver

A non-targeted LC-MS-based metabolomics approach was applied to investigate the alterations in liver metabolite levels in ALIOS diet-fed mice during the development of NAFLD. Based on the principal component analysis of the raw data (Fig. 6A), the metabolite profiles of the liver samples of ALIOS diet-fed mice were clearly distinct from those of the control mice at all time points, but no separation was observed in the samples collected at week 8, 12, and 16.

Most significantly differential metabolite features were subjected to the annotation of their identity (Fig. 6B, Supplementary Fig. S4, Supplementary Table S2). The most notable group of differential compounds was lipids. This study showed higher levels of certain phosphatidylcholines (PCs), phosphatidylethanolamines (PEs), sphingomyelins (SMs), and lysophospholipids such as lysophosphatidylcholines (LPCs), lysophosphatidylinositols (LPIs), and lysophosphatidylethanolamine (LPEs) in ALIOS diet-fed mice (Fig. 6B, Supplementary Fig. S4, Supplementary Table S2). Further, this study indicated a shift in the lipid metabolism evidenced by decrease of lipids containing polyunsaturated fatty acids such as LPE(20:5) and LPC(20:5) accompanied with increase of other lipid species such as LPI(16:0) and LPC(16:2). Some peptides such as alanyl-phenylalanine (Ala-Phe) and glutamyl-arginine (Glu-Arg) were also increased. Further, several compounds that were reduced in the liver of ALIOS diet-fed mice compared to the control mice were antioxidants including docosahexaenoic acid (DHA), eicosapentaenoic acid (EPA)-containing lipids, and alpha-tocopherol. Moreover, certain metabolites of possible gut microbial origin including LPC(15:0) and LPE(15:0) were also decreased [34,35].

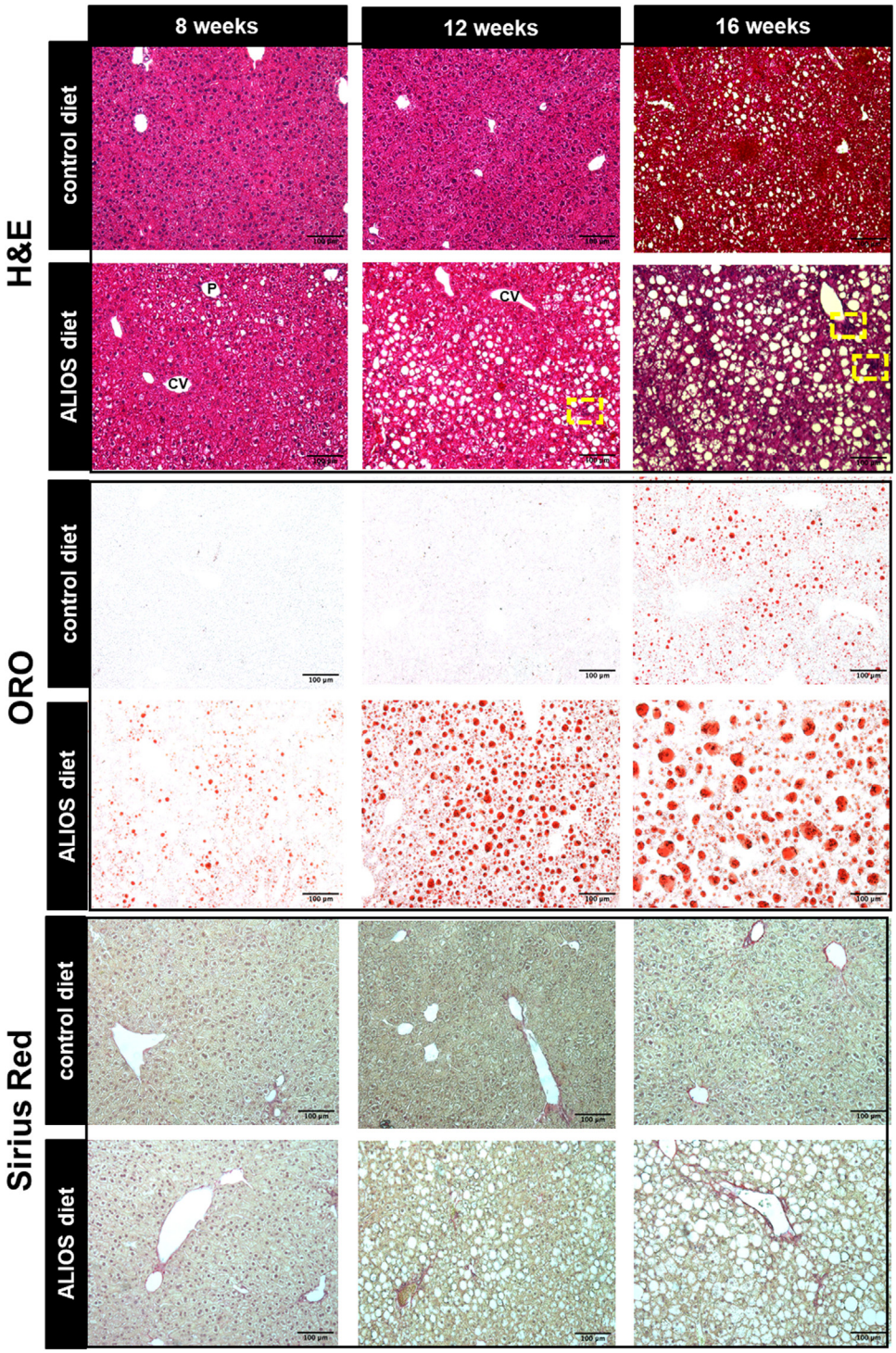

Fig. 2. ALIOS diet effects in the liver after 8, 12, and 16 weeks of diet intervention. Representative pictures of H&E, ORO, Sirius Red staining after 8, 12, and 16 weeks of ALIOS diet intervention. In H&E staining of ALIOS diet-fed mice at 12 and 16 weeks, the yellow dotted squares showed inflammatory cells scattered within the tissue, *n*=4 mice/group, 8 acquisitions/mouse, Scale bar 100 μm, 10X objective CV: central vein; P, portal tract. In ORO staining, the red droplets showed the fat droplets stained and accumulating in liver sections. Sirius Red staining, *n*=4 mice/group, 8 acquisitions/mouse, Scale bar 100 um, 10X objective. ORO: Oil Red O; ALIOS: American lifestyle-induced obesity syndrome.

3.5. Expression of genes related to inflammation and lipid metabolism was significantly correlated with changes in metabolites in the liver

To better investigate potential mechanisms governing NAFLD pathogenesis, the expression of all genes described in chapter 3.3 were further correlated with the most significantly altered liver metabolites identified in ALIOS diet-fed mice (Fig. 4 And 5, Supplementary Fig. S5).

When focusing on genes related to inflammation, we observed overall significant positive correlations with different lipids. In specific, we showed that in the earlier time point (8 weeks) of the

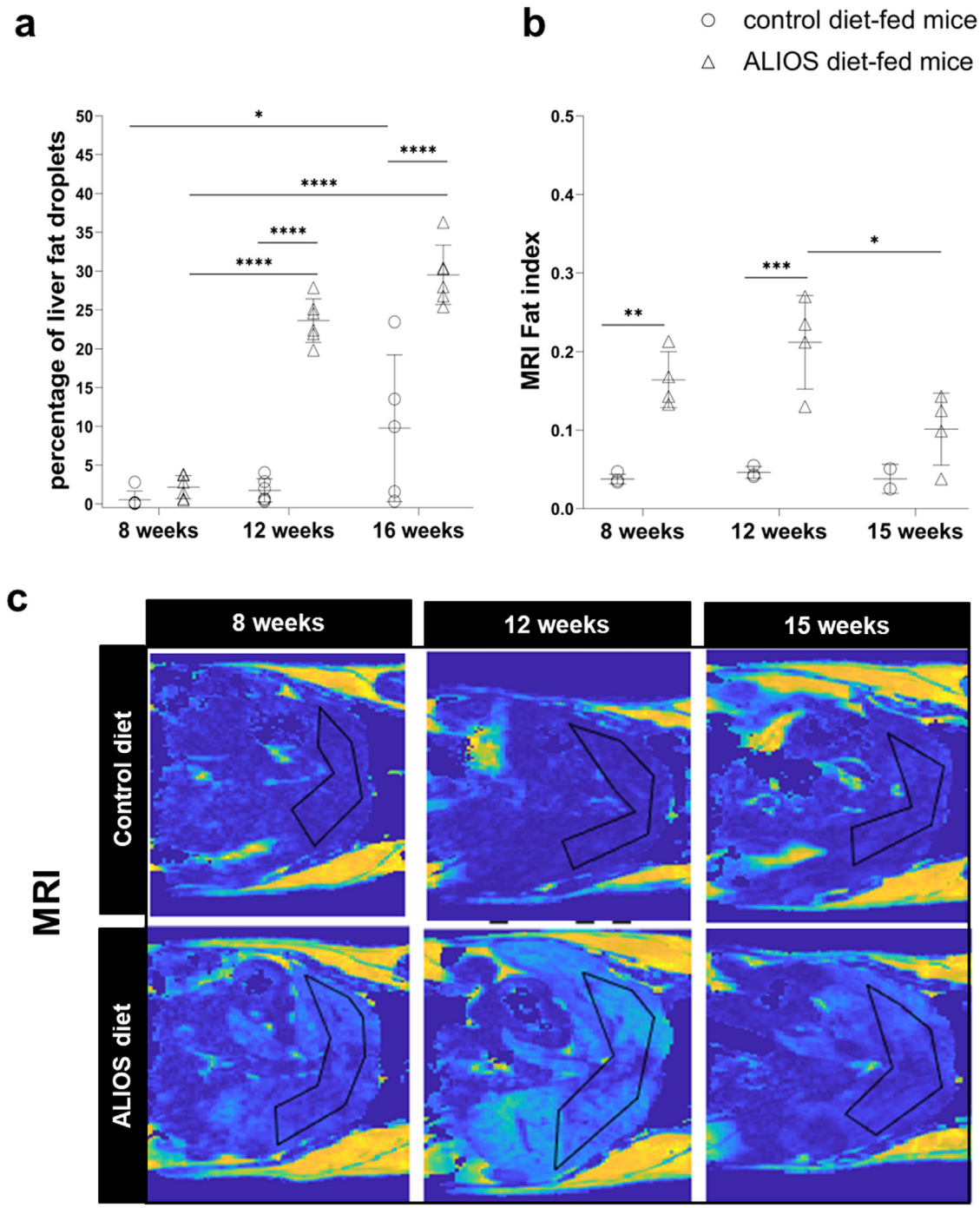

Fig. 3. ALIOS diet effects in the liver after 8, 12, and 16 weeks of diet intervention. (A) Quantitative analysis of ORO staining at 8, 12, and 16 weeks of ALIOS diet. Quantification of droplets as a percentage of total fat in the section 10X analysed, n=6 mice/group (except for control mice at week 16: n=5), 8 acquisitions/mouse, Scale bar 100 um, 10X objective. Statistical significances were shown using asterisks (* $P \leq .05$ and **** $P \leq .0001$) for inter-group comparisons at each timepoints and intra-group comparisons between different timepoints. Bar chart results were presented as average values where error bars denote SD. (B) MRI Fat index. ALIOS diet-fed mice at weeks 8 and 12 of diet intervention had significantly higher liver MRI Fat index compared to control mice, control mice (week 8: n=4; week 12: n=3; week 15: n=2); ALIOS diet-fed mice (week 8: n=4; week 12: n=4; week 15: n=4). Statistical significances were shown using asterisks (* $P \leq .05$, ** $P \leq .01$, *** $P \leq .001$) for inter-group comparisons at each timepoints and intra-group comparisons between different timepoints. Bar chart results were presented as average values where error bars denote SD. (C) Representative MRI images of livers. The location of the liver in the MRI images was indicated by the black lines. A brighter signal indicated a higher MRI fat index which means a higher liver fat content. MRI: Magnetic resonance imaging; ALIOS: American lifestyle-induced obesity syndrome.

ALIOS diet, *Tnfa* expression was positively correlated with LPCs (16:2 and 20:5) and SM(d36:2); while at 16 weeks, *Tnfa* was positively correlated with LPCs (20:5 and 20:3), LPE(18:3), LPI(16:0), and PC(42:10) (Fig. 4A-i and 4-c-i, Supplementary Fig. S5). Similarly, *Il6* gene expression was positively correlated with lipids, specifically with LPC(15:0) at 8 and 16 weeks; and with LPEs (20:5 and 22:6) at 16 weeks of the ALIOS diet. Moreover, we also reported negative correlations between *Il6* gene expression with muricholic acid and LPI(16:0) after 12 weeks of ALIOS diet and, with LPCs (18:0 and 20:4) and PC(40:6) at 16 weeks (Fig. 4B-i, Supplementary Fig. S5).

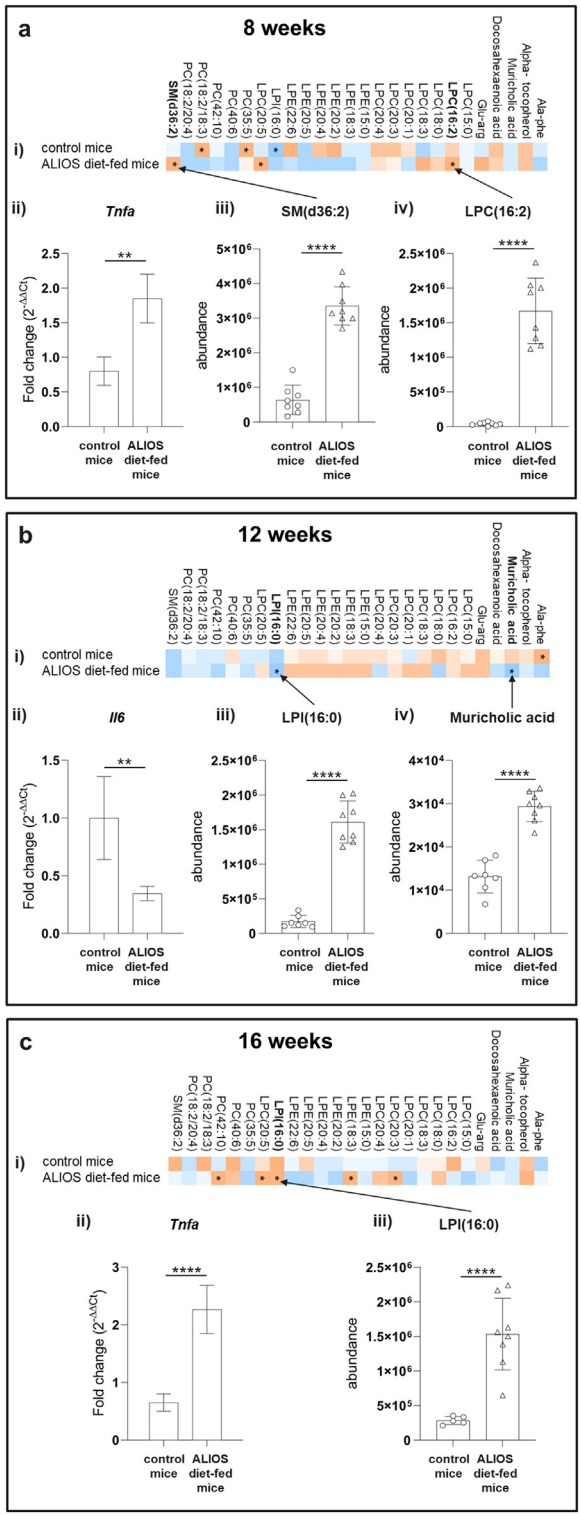

Fig. 4. Correlations between (i) significantly altered metabolites (iii & iv) and inflammatory genes (ii) in the liver during NAFLD development: at (A) 8, (B) 12 and (C) 16 weeks of ALIOS diet intervention. For heatmap and gene expression (n=4 mice/group); for metabolomics data, ALIOS diet-fed mice at week 8 (n=8), week 12 (n=8) and week 16 (n=8) and control mice at week 8 (n=8), week 12 (n=7), week 16 (n=5) of diet intervention. The intensity of the colour of the cells in the heatmaps indicates the strength of the relationship (r_s). Orange indicates a positive correlation and blue indicates a negative correlation. The cells marked with asterisks (*) demonstrate significant correlations ($P<.05$). For the bar charts, statistical significance between ALIOS diet-fed mice and control mice were shown using asterisks (** $P\leq.01$, **** $P\leq.0001$) and results are presented as average values where error bars denote SD. ALIOS, American lifestyle-induced obesity syndrome; *Il6*, Interleukin 6 gene; LPC, lysophosphatidylcholine; LPI, lysophosphatidylinositol; SM, sphingomyelin; *Tnfa*, Tumor necrosis factor alpha gene

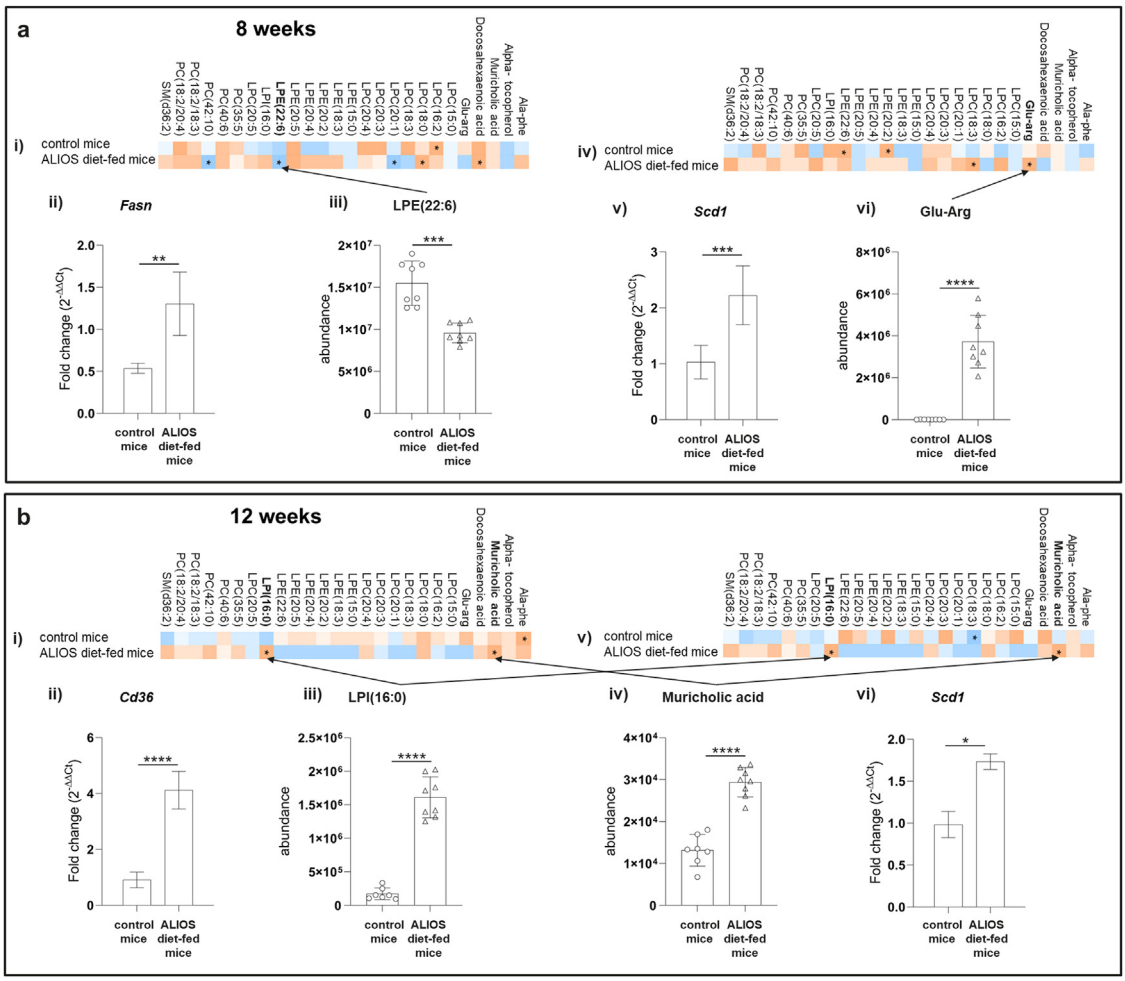

Fig. 5. Correlations (A-i-iv; B-i-v) between significantly altered metabolites (A-iii-vi; B-iii-iv) and lipid metabolism genes (A-ii-v; B-ii-vi) in the liver during NAFLD development: at (A) 8 and (B) 12 weeks of ALIOS diet intervention. For heatmap and gene expression (n=4 mice/group); for metabolomics data, ALIOS diet-fed mice at week 8 (n=8), week 12 (n=8) and week 16 (n=8) and control mice at week 8 (n=8), week 12 (n=7), week 16 (n=5) of diet intervention. The intensity of the colour of the cells in the heatmaps indicates the strength of the relationship (r_s). Orange indicates a positive correlation and blue indicates a negative correlation. The cells marked with asterisks (*) demonstrate significant correlations (P<.05). For the bar chats, statistical significance between ALIOS diet-fed mice and control mice were shown using asterisks (* P≤.05, **** P≤.0001), and results are presented as average values where error bars denote SD. ALIOS, American lifestyle-induced obesity syndrome; *Cd36*, CD36 molecule; *Fasn*, Fatty Acid Synthase; Glu-Arg, glutamyl-arginine; LPE, lysophosphatidylethanolamine; LPI, lysophosphatidylinositol; *Scd1*, Stearoyl-CoA desaturase 1

Tlr4 gene expression was positively correlated with muricholic acid at 8 weeks, LPC(18:0) at 12 weeks, as well as LPC(15:0) and LPEs (20:5 and 22:6) at 16 weeks. In addition, *Tlr4* gene expression was also negatively correlated with LPEs (20:4, 20:5, and 22:6) at week 12, and LPCs (18:0 and 20:4) and PC(40:6) at week 16 (Supplementary Fig. S5).

Among the genes related to lipid metabolism, we also found significant correlations with different lipids at different timepoints. *Cd36* expression was positively correlated with LPC(15:0) (8 weeks); muricholic acid and LPI(16:0) (12 weeks); LPC(15:0) and LPEs (20:5 and 22:6) (16 weeks). At the last timepoint (16 weeks), *Cd36* expression was negatively correlated with LPCs (18:0 and 20:4) and PC(40:6) (Fig. 5B-i, Supplementary Fig. S5). Moreover, *Acaca* expression was positively correlated with LPE(15:0) (week 8) while negatively correlated with DHA and LPC(18:3) (week 16) (Supplementary Fig. S5). At the early timepoint (8 weeks), *Fasn* expression was positively correlated with DHA and LPC(18:0) while negatively correlated with LPC(20:1), LPE(22:6), and PC(42:10) in mice fed with ALIOS diet. However, at week 16, similar to *Acaca, Fasn* expression was also negatively correlated with DHA and LPC(18:3) (Fig. 5A-i, Supplementary Fig. S5). Furthermore, we found that *Scd1* expression was correlated with different metabolites at different time points. *Scd1* expression was positively correlated with Glu-Arg and LPC(18:3) (8 weeks) as well as muricholic acid and LPI(16:0), same as *Cd36*, (12 weeks). On the other hand, *Scd1* expression was negatively correlated with LPE(20:4) (week 16; Fig. 5A-iv and 5-B-v, Supplementary Fig. S5). In addition, *Cpt1a* expression was positively correlated with LPE(20:5) (8 weeks), DHA and LPC(18:3) (16 weeks; Supplementary Fig. S5). Finally, *Ppara* expression was positively correlated with LPE(15:0) at week 8, same as *Acaca*, while also positively correlated with PC(42:10) at week 12 (Supplementary Fig. S5). We found similar correlation patterns with the same metabolites between gene expressions of *Acaca* and *Ppara* at week 8; *Cd36* and *Scd1* at week 12; *Acaca* and *Fasn* at week 16.

4. Discussion

Although the pathophysiology of NAFLD has been widely investigated, gaps remain especially in explaining how certain patients progress from NAFLD to NASH, while others do not. Therefore, understanding key players driving NAFLD pathogenesis is cru-

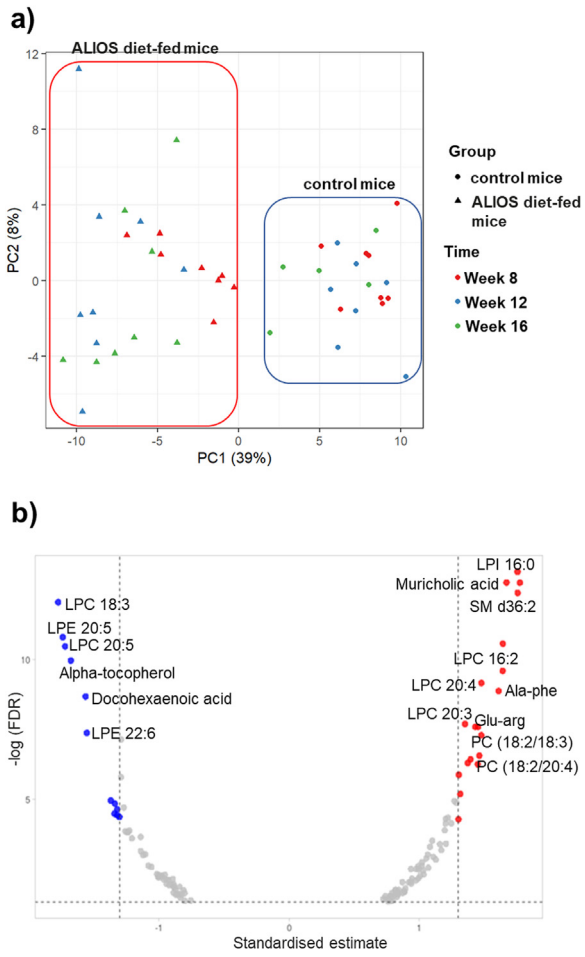

Fig. 6. Changes in hepatic metabolites between ALIOS diet-fed mice and control mice. ALIOS diet-fed mice at week 8 (n=8), week 12 (n=8) and week 16 (n=8) and control mice at week 8 (n=8), week 12 (n=7), week 16 (n=5) of diet intervention. (A) Principal component analysis (PCA) of non-targeted metabolomics data from liver samples. (B) Volcano plot of top 25 significantly different identified metabolites from the ALIOS diet intervention in the liver tissue. The data of all metabolites are plotted as the standardized estimates of the linear mixed model for the interaction between group (control mice and ALIOS diet-fed mice) and time (8, 12, and 16 weeks of the diet intervention) versus the negative logarithm of the FDR corrected *P*-values. Thresholds are shown as dashed lines. Metabolites selected as significantly increased in the ALIOS diet-fed mice are highlighted as red dots, and those that decreased significantly in the ALIOS diet-fed mice compared to the controls are shown as blue dots. Ala-phe, alanyl-phenylalanine; ALIOS, American lifestyle-induced obesity syndrome; Glu-arg, glutamyl-arginine; LPC, lysophosphatidylcholine; LPE, lysophosphatidylethanolamine; LPI, lysophosphatidylinositol; PC: phosphatidylcholine, SM, sphingomyelin.

cial and preclinical studies recapitulating the human disease progression are strongly needed for providing new mechanistic insights. In this current study, mice fed with the ALIOS diet were used to investigate the early development of NAFLD and its subsequent progression. The ALIOS diet-fed mice used in this study recapitulated NAFLD features showing higher body weight, liver mass, and energy consumption compared to the control mice which is in line with the study by Tetri et al. [15]. Moreover, mice showed an increase of fat accumulation in the liver by ORO staining at 12 and 16 weeks of the ALIOS diet compared to the controls, which was similarly reported by Mells et al. [36]. In addition, we found the expression of genes related to inflammation and lipid metabolism in the liver to be related to the lipid markers analyzed by the metabolomics analysis.

We observed changes in the expression of *Tnfa* and *Il6* genes related to inflammation. TNFα is an inflammatory cytokine that has been extensively shown to be involved with the development of NAFLD and its progression to NASH [37–39]. Indeed, the observed increase of its expression in ALIOS diet-fed mice at all time points (8, 12, and 16 weeks) in our study suggests the activation of inflammatory processes in the liver already preceding liver steatosis as also shown by Tilg and Moschen [40]. Increased expression of *Tnfa* in our study was further correlated with lipids such as SM(d36:2), LPC(16:2), and LPI(16:0), suggesting the association of the inflammatory development with changes in the lipid profile along with the fat accumulation in the liver.

Sphingolipids such as SMs and ceramides are crucial signaling molecules involved in several cellular functions [41,42] and they have been linked in promoting insulin resistance, oxidative stress, and inflammatory signaling pathways [42–44]. Moreover, higher serum levels of SMs were found in both NAFL and NASH patients [45]; SM(d36:2) has been detected in the serum samples of the NAFLD human cohort during the fibrosis stage [46]. Also, a previous study suggested that SM(d36:2) is correlated positively with *Cd68* gene expression, a biomarker of inflammation, in the liver of mice fed with western diet for 22 weeks [47] suggesting the overall importance of SMs in NAFLD progression. This is in accordance with our study, where levels of SM(d36:2) increased in ALIOS diet-fed mice in the later stage (16 weeks). However, its increase during the early stages of NAFLD (8 and 12 weeks of ALIOS diet) and its positive correlation with *Tnfa* (as observed in this study) suggests a critical role of SM(d36:2) also in NAFLD development. This finding, to the best of our knowledge has not been reported in the literature.

LPCs, in general, have been proposed as mediators of hepatic lipotoxicity [48]. LPCs have an overall increased abundance in NASH patients [11] and in the liver of both mice fed with high-fat diet (HFD) (resulting in steatosis) and in methionine-choline-deficient diet mice (developing NASH) [49]. In addition, it has been proposed that the lipotoxicity induced by LPCs may be driven by the release of proinflammatory molecules from hepatocytes stimulating the production of IL6 and IL1β in macrophages [50]. Although this may suggest a possible mechanism linking the increase of LPC(16:2) with *Tnfa* expression in our current study, the specific role of LPC(16:2) in NAFLD and its link with *Tnfa* has not yet, to our knowledge, been reported and remains to be examined. Nevertheless, increased levels of other LPCs in this study such as LPC(18:0) and LPC(20:4), which have previously been implicated in NAFLD [46,51], were also positively correlated with *Tnfa* in this study suggesting the interaction between TNFα and LPCs in promoting lipotoxicity in the hepatocytes.

Increased expression of *Tnfa* was also positively correlated with LPI(16:0) at 16 weeks of the ALIOS diet. LPI(16:0) has been found to be increased in plasma of obese [52], NAFL, and NASH patients [53] as well as mice fed with high-fat diet for 4 weeks [54]. However, as far as we know, there is no previous evidence of any correlation between LPI(16:0) with *Tnfa* in the liver samples and here we highlighted this correlation for the first time.

The role of IL6 in NAFLD development and progression is controversial [55]. In our study, at 12 weeks of ALIOS diet, mice had significantly lower *Il6* gene expression in the liver compared to the control mice. This decrease may be due to significant steatosis observed by both H&E and ORO staining at the same time point. In fact, mice lacking IL-6 were prone to develop ethanol-induced steatosis in the liver [56]. In contrast, the administration of IL-6 in high-fat diet mice alleviated hepatic steatosis [57]. The beneficial effects of IL-6 were explained by the observed increase in mitochondrial β-oxidation of fatty acid and an increase in hepatic export of triglyceride and cholesterol [57]. In fact, in

our study, *Cpt1*a was significantly highly expressed in mice fed by ALIOS diet compared to control mice after 8 weeks suggesting an increase of β-oxidation in the early stage of NAFLD. On the other hand, in our study, at 16 weeks of the ALIOS diet, the *Il6* gene expression in the liver was higher in ALIOS diet-fed mice compared to the control mice. In line with our results, Gavito et al. [58], observed an increased expression of *Il6* after 16 weeks of high fat diet in mice and IL6 administration aggravated steatosis, suggesting a detrimental role of IL6 in NAFLD progression. Furthermore, increased levels of IL6 expression have been shown in the livers of NASH patients compared to patients with steatosis or healthy liver [59] suggesting its role in NAFLD progression to NASH. In addition, IL-6 and TNF-α serum levels of obese patients and with related disorders have been correlated with adiposity [60]. The paradoxical role of *Il6* in our study remains unclear but could probably reflect different mechanisms regulating the gene expression of *Il6* depending on the site (i.e. liver or serum) and the specific metabolic context such as the different stages during NAFLD development and progression [55] as observed in our study. Furthermore, future studies at the protein levels in the liver might elucidate better the role of IL-6 in NAFLD development and progression.

The relevance of the negative correlation between *Il6* gene expression and primary bile acid muricholic acid and LPI(16:0) at 12 weeks of ALIOS diet and if muricholic acid specifically may influence *Il6* liver expression in the context of NAFLD development remains to be investigated. One possible explanation might be a suggested role of bile acid imbalances that can lead to abnormal lipid metabolism, which can be related with inflammation promoting development of NAFLD [61,62]. In accordance with our study, Li et al. [63] also showed an increase of muricholic acid in the liver of mice fed with high-fat diet for fourteen weeks. Speculative explanations might be that muricholic acid could compromise IL-6 signaling as observed in the liver of NAFLD rat model through both a caspase-mediated downregulation of gp130 and a p38(MAPK)-dependent inhibition of STAT3 phosphorylation and this may contribute to bile acid-induced hepatotoxicity [64]. In addition, it has been reported that LPIs consistently decrease several parameters of macrophage activation including IL-6 [65].

ACACA, *FASN*, and *SCD1* have been shown to be key genes involved in *de novo* lipogenesis in humans [12]. *Fasn* expression was elevated in ALIOS diet-fed mice at week 8 only. This is in line with the literature, where both mice and human studies [66] showed that gene expression of *Fasn* and *FASN* in the liver of mice and humans, respectively, was strongly associated with hepatic steatosis at the early-stage of NAFLD. Increased *Fasn* expression was negatively correlated with decreased abundance of LPE(22:6) at week 8 in ALIOS diet-fed mice in our study. Circulating levels of certain LPEs, including LPE(22:6), have been shown to be significantly reduced in NAFLD patients compared to healthy controls [45,67], which is in accordance with our study. However, the exact molecular mechanism and role of LPEs in NAFLD is still not clear [68]. A possible explanation for the reduced levels of LPE(22:6) could be due to the fatty acid side chain as we also observed a similar decrease in the abundance of LPC(22:6) in our study (data not shown).

As previously reported, SCD1 inhibition has been a target of NAFLD treatment [69,70] as hepatic SCD1 activity was increased in the NAFLD condition in humans [71]. The higher expression of *Scd1* in the ALIOS diet-fed mice compared to control mice at all time points is also in line with the literature on NAFLD mice studies [72,73]. In fact, this could mean that higher fat accumulation in the livers of the ALIOS diet-fed mice is partly due to increased *de novo* lipogenesis mediated by *Scd1* expression. In ALIOS diet-fed mice, increased *Scd1* expression was further positively correlated with increased levels of LPI(16:0). LPI(16:0) is an agonist for G protein–coupled receptor (GPR) 55 [53,74], which has been reported to be elevated in both NAFLD and NASH patients and different NAFLD animal models [53]. Fondevila et al. [53] have also demonstrated that LPIs promoted hepatic lipid accumulation through the LPI/GPR55 system by activating acetyl-CoA carboxylase (ACC). During *de novo* lipogenesis, increased ACC activity drives SCD1 activity [12] which subsequently aids the biosynthesis of triglycerides [70] leading to increased hepatic steatosis in the ALIOS diet-fed mice as seen in our study. Our results further strengthen the role of LPI(16:0) in aggravating hepatic steatosis via increased *de novo* lipogenesis.

CD36 is a fatty acid translocase involved in transporting long-chain fatty acids into hepatocytes [75,76]. In our study, it had a higher expression level in the ALIOS diet-fed mice compared to the control mice at all time points, which was in line with previous studies as shown by Rada et al. [75] and can be explained by the overload of lipids provided by the ALIOS diet. The positive correlation between increased *Cd36* and increased abundance of LPI(16:0) at week 12 in the ALIOS diet-fed mice may be due to increased uptake of LPI and/or its precursors including phosphatidylinositol (PI) [74]. Furthermore, *Cd36* (at weeks 12 and 16) and *Scd1* (at weeks 8 and 12) expressions were positively correlated with muricholic acid in the ALIOS diet-fed mice. Elevated muricholic acid can induce inactivation of Farnesoid X receptor (FXR) [77], which can subsequently increase the expression of *Cd36* and *Scd1* [78] as also observed in our study. Increased fat uptake and lipid synthesis mediated by elevated expressions of *Cd36* and *Scd1,* respectively, thus led to increased lipid accumulation in the liver [12] found in our ALIOS diet-fed mice.

Oxidative stress has been shown to play a role in NAFLD, and unbalanced antioxidant status in the liver contributes to the pathogenesis and progression of NAFLD to NASH [79]. In our study, we observed a reduced abundance of antioxidants such as alpha-tocopherol, DHA, and EPA-containing lipids at all time points in the ALIOS diet-fed mice. Indeed, the abundance of C_{20-22} omega-3 polyunsaturated fatty acids (including DHA and EPA) and alpha-tocopherol were found to be lower in NAFLD and NASH patients as well as in NAFLD mouse models [80,81]. The reduction of antioxidant compounds found in our study may suggest an accumulation of ROS leading to liver injury [82,83] and contributing to NAFLD development and progression.

Furthermore, increased *Scd1* expression was positively correlated with increased abundance of Glu-Arg in the ALIOS diet-fed mice observed at week 8. The levels of γ-Glu-Arg in the serum of NAFLD patients were higher compared to healthy control but also higher in simple steatosis compared to NASH [84]. Our results were consistent with the literature where in the liver, the abundance of Glu-Arg in the ALIOS diet-fed mice was statistically higher than the control mice at all timepoints. The generation of γ-glutamyl dipeptides is a result of being a by-product in the synthesis of reduced glutathione (GSH) [84] to neutralize the ROS generated during NAFLD. It acts as a protective mechanism to attenuate NAFLD progression, resulting in the high levels of γ-glutamyl dipeptides in NAFLD. However, GSH synthesis is reduced due to limited accessibility to glycine in the NAFLD condition [85]. Eventually, production exceeds the capacity of GSH synthesis resulting in increased oxidative stress and progression to NASH [84]. These results are similar to our findings where the abundance of Glu-Arg gradually decreased in the ALIOS diet-fed mice with a statistically significant reduction from week 8 to 12 and 16. The correlation between *Scd1* expression and Glu-Arg abundance also turned from positive (week 8) to negative (weeks 12 and 16). Reduced capacity to neutralize oxidative processes as indicated by the lowering of the Glu-Arg abundance in the ALIOS diet-fed mice may be a driving force for

NAFLD progression and increased hepatic steatosis via *de novo* lipogenesis.

Due to the close anatomical structure between the gut and the liver via the portal vein that form the gut-liver axis, changes in the composition and functions of gut microbiota and their metabolites have been shown to contribute towards NAFLD development and progression [86,87]. In our study, we observed a reduction of two long, odd-chain fatty acids, namely LPC(15:0) and LPE(15:0) in the livers of ALIOS-diet fed mice, which are linked to the gut microbiota [35,88]. Fecal and circulating LPCs and LPEs in general have previously been associated with several bacterial species in the gut [89–91]. In line with our study, LPC(15:0) was decreased in plasma of 12 week high fat fed mice [92]. LPC(15:0) has been known to confer protection from diabetes by inducing insulin secretion, thereby reducing glucose levels [34]. The reduction of these beneficial gut-derived metabolites in our study may suggest an induction of insulin resistance, thereby causing NAFLD progression. In addition, the altered gut microbiota-derived metabolites might also lead to an increased risk of developing diabetes, a comorbidity of NAFLD [89–91].

5. Conclusions

As the pathophysiology of NAFLD is poorly understood, taking advantage of the combination of non-targeted metabolomics and gene expression with biochemical findings, our study provides further insights into the mechanistic events occurring in the liver in NAFLD development and progression. The ALIOS diet-fed mice developed NAFLD along with marked differences in liver metabolite abundance, most evident changes observed in the reduction of lipids with polyunsaturated fatty acids alongside increase in other lipid species. The expression of some inflammation-related genes varied along the disease progression and exhibited varying correlation with the differential metabolite levels. Specifically, elevated SM(d36:2), LPC(16:2), LPI(16:0) might promote inflammation via elevated *Tnfa*. Increased hepatic inflammation drives NAFLD development and progression to NASH. This can be aggravated by the reduction of antioxidant metabolites observed in our study. A combination of increased lipid uptake and fat synthesis is responsible for the hepatic steatosis during NAFLD development and progression. In fact, we observed increased levels of LPI(16:0) and muricholic acid drive liver fat uptake by increasing *Cd36* expression. Reduced levels of LPE(22:6) together with increased levels of Glu-Arg, LPI(16:0), and muricholic acid drive fat synthesis via increasing *Fasn* and *Scd1* expression. Decreased levels of gut microbiota-derived lipids might further contribute towards NAFLD development and progression. The combination of non-targeted metabolomics data with gene expression in future studies can further identify the key metabolic routes during NAFLD development and progression. These metabolic routes could be the targets of potential novel therapeutic approaches for NAFLD.

Author Contributions

The authors confirm contribution to the paper as follows: study conception and design: V.I., J.L., C.G.G., A. Kårlund, M. Kolehmainen, and H.E. Data collection: V.I., J.L., A.F.B. and C.G.G. Analysis and interpretation of results: V.I., J.L., A.F.B., C.G.G., R.M.W., M. Kettunen, A. Klåvus, U.S., V.K., M. Kolehmainen, K.H. and H.E. Draft manuscript preparation: A.F.B., J.L., and V.I. drafted the first version of the manuscript under the supervision of C.G.G., H.E., K.H., and M.Kolehmainen. All authors read, reviewed, and approved the final manuscript. Funding acquisition: U.S. coordinated the programme under the Marie Skłodowska-Curie grant agreement No 813781 at the University of Eastern Finland (Kuopio, Finland). V.I., J.L., and A.F.B. contributed equally.

Declaration of Competing Interest

The authors have no relevant conflict of interest to disclose.

Ambrin Farizah Babu, Ville Koistinen, Anton Klåvus, and Kati Hanhineva are employed by Afekta Technologies Ltd. The remaining authors declare that the research was conducted in the absence of any commercial or financial relationships that could be construed as a potential conflict of interest.

Acknowledgment

Miia Reponen is thanked for running the samples in the LC-MS instrument. Anne Koivisto is also thanked for providing training and enabling the usage of the histochemistry facility. Part of the work was carried out with the support of the Kuopio Biomedical Imaging Unit, University of Eastern Finland, Kuopio, Finland (part of Finnish Biomedical Imaging Node, EuroBioImaging). The graphical abstract was made in part using BioRender (BioRender—biorender.com).

Funding

This work was supported by the ITN Marie Curie BestTreat-Building a Gut Microbiome Engineering Toolbox for In Situ Therapeutic Treatments for Non-alcoholic Fatty Liver Disease (grant number 813781).

Supplementary materials

Supplementary material associated with this article can be found, in the online version, at doi:10.1016/j.jnutbio.2023.109307.

References

[1] Cotter TG, Rinella M. Nonalcoholic fatty liver disease 2020: the state of the disease. Gastroenterology 2020;158:1851–64.
[2] Angulo P. Nonalcoholic fatty liver disease. N Engl J Med 2002;346:1221–31.
[3] Farrell GC, Larter CZ. Nonalcoholic fatty liver disease: from steatosis to cirrhosis. Hepatology 2006;43:S99–S112.
[4] Byrne CD, Targher G. NAFLD: a multisystem disease. J Hepatol 2015;62:S47–64.
[5] Younossi ZM, Koenig AB, Abdelatif D, Fazel Y, Henry L, Wymer M. Global epidemiology of nonalcoholic fatty liver disease—meta-analytic assessment of prevalence, incidence, and outcomes. Hepatology 2016;64:73–84.
[6] Tiniakos D, Vos M, Brunt E. Nonalcoholic steatohepatitis: pathology and pathophysiology. Ann Rev Pathol 2010;5:145–71.
[7] Canfora EE, Meex RC, Venema K, Blaak EE. Gut microbial metabolites in obesity, NAFLD and T2DM. Nat Rev Endocrinol 2019;15:261–73.
[8] Buckley J. Availability of high-fat foods might drive the obesity epidemic. Nat Rev Endocrinol 2018;14:574–5.
[9] Lai Y-S, Chen W-C, Kuo T-C, Ho C-T, Kuo C-H, Tseng YJ, et al. Mass-spectrometry-based serum metabolomics of a C57BL/6J mouse model of high-fat-diet-induced non-alcoholic fatty liver disease development. J Agric Food Chem 2015;63:7873–84.
[10] Araya J, Rodrigo R, Videla LA, Thielemann L, Orellana M, Pettinelli P, et al. Increase in long-chain polyunsaturated fatty acid n− 6/n− 3 ratio in relation to hepatic steatosis in patients with non-alcoholic fatty liver disease. Clin Sci (Colch) 2004;106:635–43.
[11] Puri P, Baillie RA, Wiest MM, Mirshahi F, Choudhury J, Cheung O, et al. A lipidomic analysis of nonalcoholic fatty liver disease. Hepatology 2007;46:1081–90.
[12] Ipsen DH, Lykkesfeldt J, Tveden-Nyborg P. Molecular mechanisms of hepatic lipid accumulation in non-alcoholic fatty liver disease. Cell Mol Life Sci 2018;75:3313–27.
[13] Harris SE, Poolman TM, Arvaniti A, Cox RD, Gathercole LL, Tomlinson JW. The American lifestyle-induced obesity syndrome diet in male and female rodents recapitulates the clinical and transcriptomic features of nonalcoholic fatty liver disease and nonalcoholic steatohepatitis. Am J Physiol-Gastrointest Liver Physiol 2020;319:G345–GG60.
[14] Percie du Sert N, Hurst V, Ahluwalia A, Alam S, Avey M, Baker M, et al. The ARRIVE guidelines 2.0: Updated guidelines for reporting animal research. PLoS Biol 2020;18:e3000410.

[15] Tetri LH, Basaranoglu M, Brunt EM, Yerian LM, Neuschwander-Tetri BA. Severe NAFLD with hepatic necroinflammatory changes in mice fed trans fats and a high-fructose corn syrup equivalent. Am J Physiol Gastrointest Liver Physiol 2008;295:G987–95.
[16] Faul F, Erdfelder E, Lang AG, Buchner A. G*Power 3: a flexible statistical power analysis program for the social, behavioral, and biomedical sciences. Behav Res Methods 2007;39:175–91.
[17] Faul F, Erdfelder E, Buchner A, Lang AG. Statistical power analyses using G*Power 3.1: tests for correlation and regression analyses. Behav Res Methods 2009;41:1149–60.
[18] Schumann G, Bonora R, Ceriotti F, Férard G, Ferrero CA, Franck PF, et al. IFCC primary reference procedures for the measurement of catalytic activity concentrations of enzymes at 37 degrees C. Part 5. Reference procedure for the measurement of catalytic concentration of aspartate aminotransferase. Clin Chem Lab Med. 2002;40(7):725–33.
[19] Schumann G, Bonora R, Ceriotti F, Férard G, Ferrero CA, Franck PF, et al. IFCC primary reference procedures for the measurement of catalytic activity concentrations of enzymes at 37 degrees C. Part 4. Reference procedure for the measurement of catalytic concentration of alanine aminotransferase. Clin Chem Lab Med 2002;40(7):718–24.
[20] Pirinen E, Kuulasmaa T, Pietilä M, Heikkinen S, Tusa M, Itkonen P, et al. Enhanced polyamine catabolism alters homeostatic control of white adipose tissue mass, energy expenditure, and glucose metabolism. Mol Cell Biol 2007;27:4953–67.
[21] Medina-Gomez G, Virtue S, Lelliott C, Boiani R, Campbell M, Christodoulides C, et al. The link between nutritional status and insulin sensitivity is dependent on the adipocyte-specific peroxisome proliferator–activated receptor-γ2 isoform. Diabetes 2005;54:1706–16.
[22] Liang W, Menke AL, Driessen A, Koek GH, Lindeman JH, Stoop R, et al. Establishment of a general NAFLD scoring system for rodent models and comparison to human liver pathology. PLoS One 2014;9:e115922.
[23] Arganda-Carreras I, Kaynig V, Rueden C, Eliceiri KW, Schindelin J, Cardona A, et al. Trainable Weka Segmentation: a machine learning tool for microscopy pixel classification. Bioinformatics 2017;33:2424–6.
[24] Livak KJ, Schmittgen TD. Analysis of relative gene expression data using real–time quantitative PCR and the 2− ΔΔCT method. Methods 2001;25:402–8.
[25] Klåvus A, Kokla M, Noerman S, Koistinen VM, Tuomainen M, Zarei I, et al. "Notame": workflow for non-targeted LC–MS metabolic profiling. Metabolites 2020;10:135.
[26] Tsugawa H, Cajka T, Kind T, Ma Y, Higgins B, Ikeda K, et al. MS-DIAL: data-independent MS/MS deconvolution for comprehensive metabolome analysis. Nat Methods 2015;12:523–6.
[27] Broadhurst D, Goodacre R, Reinke SN, Kuligowski J, Wilson ID, Lewis MR, et al. Guidelines and considerations for the use of system suitability and quality control samples in mass spectrometry assays applied in untargeted clinical metabolomic studies. Metabolomics 2018;14:1–17.
[28] R Core Team. R: A language and environment for statistical computing. R foundation for statistical computing, Vienna, Austria 2020.
[29] Horai H, Arita M, Kanaya S, Nihei Y, Ikeda T, Suwa K, et al. MassBank: a public repository for sharing mass spectral data for life sciences. J Mass Spectrom. 2010 Jul;45(7):703–714. Date of access: July 11, 2022.
[30] The LIPID MAPS® Lipidomics Gateway, https://www.lipidmaps.org/.
[31] Smith CA, O'Maille G, Want EJ, Qin C, Trauger SA, Brandon TR, et al. METLIN: a metabolite mass spectral database. Ther Drug Monit 2005;27:747–51.
[32] Wishart D, Tzur D, Knox C. HMDB: the Human Metabolome Database. Nucleic Acids Res. 2007 Jan;35(Database issue):D521-6
[33] Tsugawa H, Kind T, Nakabayashi R, Yukihira D, Tanaka W, Cajka T, et al. Hydrogen rearrangement rules: computational MS/MS fragmentation and structure elucidation using MS-FINDER software. Anal Chem 2016;88:7946–58.
[34] De Mello VD, Paananen J, Lindström J, Lankinen MA, Shi L, Kuusisto J, et al. Indolepropionic acid and novel lipid metabolites are associated with a lower risk of type 2 diabetes in the finnish diabetes prevention study. Sci Rep 2017;7:1–12.
[35] Lee T, Clavel T, Smirnov K, Schmidt A, Lagkouvardos I, Walker A, et al. Oral versus intravenous iron replacement therapy distinctly alters the gut microbiota and metabolome in patients with IBD. Gut 2017;66:863–71.
[36] Mells JE, Fu PP, Sharma S, Olson D, Cheng L, Handy JA, et al. Glp-1 analog, liraglutide, ameliorates hepatic steatosis and cardiac hypertrophy in C57BL/6J mice fed a Western diet. Am J Physiol-Gastroint Liver Physiol 2012;302:G225–GG35.
[37] Kakino S, Ohki T, Nakayama H, Yuan X, Otabe S, Hashinaga T, et al. Pivotal role of TNF-α in the development and progression of nonalcoholic fatty liver disease in a murine model. Horm Metab Res 2018;50:80–7.
[38] Wandrer F, Liebig S, Marhenke S, Vogel A, John K, Manns MP, et al. TNF-Receptor-1 inhibition reduces liver steatosis, hepatocellular injury and fibrosis in NAFLD mice. Cell Death Dis 2020;11:1–9.
[39] Crespo J, Fern P, Hern M, Mayorga M, Pons-Romero F. Gene expression of tumor necrosis factor [alpha] and TNF-receptors, p55 and p75, in nonalcoholic steatohepatitis patients. Hepatology 2001;34:1158–63.
[40] Tilg H, Moschen AR. Evolution of inflammation in nonalcoholic fatty liver disease: the multiple parallel hits hypothesis. Hepatology 2010;52:1836–46.
[41] Marí M, Fernández-Checa JC. Sphingolipid signalling and liver diseases. Liver Int 2007;27:440–50.
[42] Maceyka M, Spiegel S. Sphingolipid metabolites in inflammatory disease. Nature 2014;510:58–67.
[43] Bikman BT. A role for sphingolipids in the pathophysiology of obesity-induced inflammation. Cell Mol Life Sci 2012;69:2135–46.
[44] Chavez JA, Siddique MM, Wang ST, Ching J, Shayman JA, Summers SA. Ceramides and glucosylceramides are independent antagonists of insulin signaling. J Biol Chem 2014;289:723–34.
[45] Tiwari-Heckler S, Gan-Schreier H, Stremmel W, Chamulitrat W, Pathil A. Circulating phospholipid patterns in NAFLD patients associated with a combination of metabolic risk factors. Nutrients 2018;10:649.
[46] McGlinchey AJ, Govaere O, Geng D, Ratziu V, Allison M, Bousier J, et al. Metabolic signatures across the full spectrum of nonalcoholic fatty liver disease. JHEP Rep 2022;4.
[47] García-Jaramillo M, Lytle KA, Spooner MH, Jump DB. A lipidomic analysis of docosahexaenoic acid (22: 6, ω3) mediated attenuation of western diet induced nonalcoholic steatohepatitis in male ldlr-/-mice. Metabolites 2019;9:252.
[48] Han MS, Park SY, Shinzawa K, Kim S, Chung KW, Lee J-H, et al. Lysophosphatidylcholine as a death effector in the lipoapoptosis of hepatocytess. J Lipid Res 2008;49:84–97.
[49] Pathil A, Mueller J, Warth A, Chamulitrat W, Stremmel W. Ursodeoxycholyl lysophosphatidylethanolamide improves steatosis and inflammation in murine models of nonalcoholic fatty liver disease. Hepatology 2012;55:1369–78.
[50] Hirsova P, Ibrahim SH, Krishnan A, Verma VK, Bronk SF, Werneburg NW, et al. Lipid-induced signaling causes release of inflammatory extracellular vesicles from hepatocytes. Gastroenterology 2016;150:956–67.
[51] Tanaka N, Matsubara T, Krausz KW, Patterson AD, Gonzalez FJ. Disruption of phospholipid and bile acid homeostasis in mice with nonalcoholic steatohepatitis. Hepatology 2012;56:118–29.
[52] Moreno-Navarrete JM, Catalán V, Whyte L, Díaz-Arteaga A, Vázquez–Martínez R, et al. The L-α-lysophosphatidylinositol/GPR55 system and its potential role in human obesity. Diabetes 2012;61:281–91.
[53] Fondevila MF, Fernandez U, Gonzalez-Rellan MJ, Da Silva Lima N, Buque X, Gonzalez-Rodriguez A, et al. The L-α-Lysophosphatidylinositol/G Protein–Coupled Receptor 55 System Induces the Development of Nonalcoholic Steatosis and Steatohepatitis. Hepatology 2021;73:606–24.
[54] Kang S, Lee A-Y, Park S-Y, Liu K-H, Im D-S. O-1602 Promotes Hepatic Steatosis through GPR55 and PI3 Kinase/Akt/SREBP-1c Signaling in Mice. Int J Mol Sci 2021;22:3091.
[55] Beuchler C, Bauer S. IL-6 in non-alcoholic fatty liver disease-good, evil or both. Endocrinol Metabolic Syndrome 2011;1:1–3.
[56] El-Assal O, Hong F, Kim W-H, Radaeva S, Gao B. IL-6-deficient mice are susceptible to ethanol-induced hepatic steatosis: IL-6 protects against ethanol-induced oxidative stress and mitochondrial permeability transition in the liver. Cell Mol Immunol 2004;1:205–11.
[57] Hong F, Radaeva S, Pan HN, Tian Z, Veech R, Gao B. Interleukin 6 alleviates hepatic steatosis and ischemia/reperfusion injury in mice with fatty liver disease. Hepatology 2004;40:933–41.
[58] Gavito AL, Bautista D, Suarez J, Badran S, Arco R, Pavón FJ, et al. Chronic IL-6 administration desensitizes IL-6 response in liver, causes hyperleptinemia and aggravates steatosis in diet-induced-obese mice. PLoS One 2016;11:e0157956.
[59] Wieckowska A, Papouchado BG, Li Z, Lopez R, Zein NN, Feldstein AE. Increased hepatic and circulating interleukin-6 levels in human nonalcoholic steatohepatitis. J AM College Gastroenterol| ACG 2008;103:1372–9.
[60] Popko K, Gorska E, Stelmaszczyk-Emmel A, Plywaczewski R, Stoklosa A, Gorecka D, et al. Proinflammatory cytokines Il-6 and TNF-α and the development of inflammation in obese subjects. Eur J Med Res 2010;15:1–3.
[61] Li Y, Jadhav K, Zhang Y. Bile acid receptors in non-alcoholic fatty liver disease. Biochem Pharmacol 2013;86:1517–24.
[62] Yuan L, Bambha K. Bile acid receptors and nonalcoholic fatty liver disease. World J Hepatol 2015;7:2811.
[63] Li H, Xi Y, Xin X, Tian H, Hu Y. Gypenosides regulate farnesoid X receptor–mediated bile acid and lipid metabolism in a mouse model of non-alcoholic steatohepatitis. Nutr Metab (Lond) 2020;17:1–15.
[64] Graf D, Kohlmann C, Haselow K, Gehrmann T, Bode JG, Häussinger D. Bile acids inhibit interleukin-6 signaling via gp130 receptor-dependent and-independent pathways in rat liver. Hepatology 2006;44:1206–17.
[65] Masquelier J, Alhouayek M, Terrasi R, Bottemanne P, Paquot A, Muccioli GG. Lysophosphatidylinositols in inflammation and macrophage activation: Altered levels and anti-inflammatory effects. Molecul Cell Biol Lipids 2018;1863:1458–68.
[66] Dorn C, Riener M-O, Kirovski G, Saugspier M, Steib K, Weiss TS, et al. Expression of fatty acid synthase in nonalcoholic fatty liver disease. Int J Clin Exp Pathol 2010;3:505.
[67] Yamamoto Y, Sakurai T, Chen Z, Furukawa T, Gowda SGB, Wu Y, et al. Analysis of serum lysophosphatidylethanolamine levels in patients with non-alcoholic fatty liver disease by liquid chromatography-tandem mass spectrometry. Anal BioanalChem 2021;413:245–54.
[68] Draijer LG, Froon-Torenstra D, van Weeghel M, Vaz FM, Bohte AE, Holleboom AG, et al. Lipidomics in nonalcoholic fatty liver disease: exploring serum lipids as biomarkers for pediatric nonalcoholic fatty liver disease. J Pediatr Gastroenterol Nutr 2020;71:433–9.
[69] Ferguson D, Finck BN. Emerging therapeutic approaches for the treatment of NAFLD and type 2 diabetes mellitus. Nat Rev Endocrinol 2021;17:484–495.

[70] Jeyakumar SM, Vajreswari A. Stearoyl-CoA desaturase 1: A potential target for non-alcoholic fatty liver disease?-perspective on emerging experimental evidence. World J Hepatol 2022;14:168.
[71] Kotronen A, Seppänen-Laakso T, Westerbacka J, Kiviluoto T, Arola J, Ruskeepää A-L, et al. Hepatic stearoyl-CoA desaturase (SCD)-1 activity and diacylglycerol but not ceramide concentrations are increased in the nonalcoholic human fatty liver. Diabetes 2009;58:203–8.
[72] Rao A, Kosters A, Mells JE, Zhang W, Setchell KD, Amanso AM, et al. Inhibition of ileal bile acid uptake protects against nonalcoholic fatty liver disease in high-fat diet–fed mice. Sci Transl Med 2016 Sep 21;8(357):357ra122.
[73] Biddinger SB, Almind K, Miyazaki M, Kokkotou E, Ntambi JM, Kahn CR. Effects of diet and genetic background on sterol regulatory element-binding protein-1c, stearoyl-CoA desaturase 1, and the development of the metabolic syndrome. Diabetes 2005;54:1314–23.
[74] Yamashita A, Oka S, Tanikawa T, Hayashi Y, Nemoto-Sasaki Y, Sugiura T. The actions and metabolism of lysophosphatidylinositol, an endogenous agonist for GPR55. Prostaglandins Other Lipid Mediat 2013;107:103–16.
[75] Rada P, González-Rodríguez Á, García-Monzón C, Valverde ÁM. Understanding lipotoxicity in NAFLD pathogenesis: is CD36 a key driver? Cell Death Dis 2020;11:1–15.
[76] Pei K, Gui T, Kan D, Feng H, Jin Y, Yang Y, et al. An overview of lipid metabolism and nonalcoholic fatty liver disease. Biomed Res Int. 2020 Jul 18;2020:4020249.
[77] Jiang L, Zhang H, Xiao D, Wei H, Chen Y. Farnesoid X receptor (FXR): Structures and ligands. Comput Structu Biotechnol J 2021;19:2148–59.
[78] Xi Y, Li H. Role of farnesoid X receptor in hepatic steatosis in nonalcoholic fatty liver disease. Biomed Pharmacother 2020;121:109609.
[79] Arroyave-Ospina JC, Wu Z, Geng Y, Moshage H. Role of oxidative stress in the pathogenesis of non-alcoholic fatty liver disease: Implications for prevention and therapy. Antioxidants 2021;10:174.
[80] Spooner MH, Jump DB. Omega-3 fatty acids and nonalcoholic fatty liver disease in adults and children: where do we stand? Curr Opin Clin Nutr Metab Care 2019;22:103.
[81] Pacana T, Sanyal AJ. Vitamin E and non-alcoholic fatty liver disease. Curr Opin Clin Nutr Metab Care 2012;15:641.
[82] Rolo AP, Teodoro JS, Palmeira CM. Role of oxidative stress in the pathogenesis of nonalcoholic steatohepatitis. Free Radical Biol Med 2012;52:59–69.
[83] Serviddio G, Bellanti F, Vendemiale G. Free radical biology for medicine: learning from nonalcoholic fatty liver disease. Free Radical Biol Med 2013;65:952–68.
[84] Soga T, Sugimoto M, Honma M, Mori M, Igarashi K, Kashikura K, et al. Serum metabolomics reveals γ-glutamyl dipeptides as biomarkers for discrimination among different forms of liver disease. J Hepatol 2011;55:896–905.
[85] Rom O, Liu Y, Liu Z, Zhao Y, Wu J, Ghrayeb A, et al. Glycine-based treatment ameliorates NAFLD by modulating fatty acid oxidation, glutathione synthesis, and the gut microbiome. Sci Transl Med 2020;12:eaaz2841.
[86] Zhou J, Tripathi M, Sinha RA, Singh BK, Yen PM Gut microbiota and their metabolites in the progression of non-alcoholic fatty liver disease. Hepatoma Res 2021 Jan 13;7:11.
[87] Han H, Jiang Y, Wang M, Melaku M, Liu L, Zhao Y, et al. Intestinal dysbiosis in nonalcoholic fatty liver disease (NAFLD): Focusing on the gut–liver axis. Crit Rev Food Sci Nutr Aug 2021;18:1–18.
[88] Lahti L, Salonen A, Kekkonen RA, Salojärvi J, Jalanka-Tuovinen J, Palva A, et al. Associations between the human intestinal microbiota, Lactobacillus rhamnosus GG and serum lipids indicated by integrated analysis of high-throughput profiling data. PeerJ 2013;1:e32.
[89] Wang Z, Peters BA, Usyk M, Xing J, Hanna DB, Wang T, et al. Gut microbiota, plasma metabolomic profiles, and carotid artery atherosclerosis in HIV infection. Arterioscler Thromb Vasc Biol. 2022;42(8):1081–93.
[90] Shao J, Liu Y, Wang H, Luo Y, Chen L. An integrated fecal microbiome and metabolomics in T2DM rats reveal antidiabetes effects from host-microbial metabolic Axis of EtOAc extract from Sophora flavescens. Oxid Med Cell Longev. 2020;27:1805418.
[91] Watanabe Y, Fujisaka S, Ikeda K, Ishikawa M, Yamada T, Nawaz A, et al. Gut microbiota, determined by dietary nutrients, drive modification of the plasma lipid profile and insulin resistance. Iscience 2021;24:102445.
[92] Barber MN, Risis S, Yang C, Meikle PJ, Staples M, Febbraio MA, et al. Plasma lysophosphatidylcholine levels are reduced in obesity and type 2 diabetes. PLoS One 2012;7:e41456.